

Edge Modes, Degeneracies, and Topological Numbers in Non-Hermitian Systems

Daniel Leykam,¹ Konstantin Y. Bliokh,^{2,3} Chunli Huang,^{1,4} Y. D. Chong,^{1,5} and Franco Nori^{2,6}

¹*Division of Physics and Applied Physics, School of Physical and Mathematical Sciences, Nanyang Technological University, Singapore 637371, Singapore*

²*CEMS, RIKEN, Wako-shi, Saitama 351-0198, Japan*

³*Nonlinear Physics Centre, RSPE, The Australian National University, Canberra, ACT 0200, Australia*

⁴*Department of Physics, National Tsing Hua University, Hsinchu 30013, Taiwan*

⁵*Centre for Disruptive Photonic Technologies, Nanyang Technological University, Singapore, 637371, Singapore*

⁶*Physics Department, University of Michigan, Ann Arbor, Michigan 48109-1040, USA*

We analyze chiral topological edge modes in a non-Hermitian variant of the 2D Dirac equation. Such modes appear at interfaces between media with different “masses” and/or signs of the “non-Hermitian charge”. The appearance and regions of existence of the edge modes are intimately related to *exceptional points*, i.e., degeneracies in the bulk spectra of the media. We find that the topological edge modes can be divided into *three classes* (“Hermitian-like”, “non-Hermitian”, and “mixed”), and these are described by *two winding numbers* corresponding to a pair of half-integer charges carried by exceptional points of the bulk Hamiltonian. We also show that the non-Hermitian topological edge modes can be realized in a honeycomb-like lattice of ring resonators with non-Hermitian couplings.

Introduction. — There is presently enormous interest in two groups of fundamental physical phenomena: (i) topological edge modes in quantum Hall fluids and topological insulators [1], which are Hermitian, and (ii) novel effects in non-Hermitian wave systems (including PT-symmetric systems) [2]. Both types of phenomena have been studied in the context of quantum as well as classical waves, and both are deeply tied to the geometrical features of spectral degeneracies. In the Hermitian case, the common degeneracies are Dirac points: linear band-crossings (generically, in a 3D parameter space), which separate distinct topological phases and mark the birth or destruction of topological edge modes [3]. Non-Hermitian systems, however, exhibit a distinct class of spectral degeneracies known as *exceptional points* (EPs), which are branch points in a 2D parameter space where the Hamiltonian becomes non-diagonalizable [4].

In Hermitian systems, the bulk-edge correspondence relations that give rise to topological edge modes are typically based upon the Berry connection, which in turn relies on the eigenvector orthogonality granted by Hermiticity [1]. Is there a generalization of the bulk-edge correspondence to non-Hermitian systems [5]? When sufficiently weak non-Hermiticity (e.g. loss) is introduced to topological insulator models, the edge modes can retain some of their original characteristics [6, 7]. On the other hand, certain non-Hermitian models with chiral symmetry can support anomalous edge modes that have no clear relationship to Hermitian topological edge modes [8, 9]. These modes are embedded within a complex gapless band structure, and appear in the vicinity of EPs; however, it is not known whether they can be related to model-independent bulk topological invariants similar to those in Hermitian systems.

This paper aims to shed light on the nature of topological edge modes in non-Hermitian quantum systems.

In contrast to previous studies based on lattice models [5–10], here we focus on a non-Hermitian *continuum* model. This is motivated by the fact that, in the Hermitian case, many model-independent features of topological edge modes can be understood in terms of the generic properties of continuum models, such as the Dirac equation in various dimensions [11, 12]. For example, zero-energy Jackiw-Rebbi end modes of the 1D Dirac equation [11] unperpin end modes of the SSH lattice model [13].

Our continuum model consists of a 2D non-Hermitian Hamiltonian that is linear in both k_x and k_y and possesses a tunable mass parameter m , similar to the 2D Dirac equation. The bulk band structure is complex and possesses a pair of EPs (branch points). Along interfaces between media with different “masses” and/or signs of the non-Hermiticity, we find that there exist *zero-energy chiral edge modes*. Remarkably, the appearance of these edge modes and their regions of existence are fully determined by the EPs in the bulk spectra of the media. We show that these modes can be classified as “Hermitian-like”, “non-Hermitian”, and “mixed”, using *two topological numbers*. The first number is related to the chirality of the eigenstates (i.e., the sign of the Berry curvature), while the second one characterizes the chirality of the EP. The “non-Hermitian” and “mixed” edge modes resemble the “anomalous” edge modes found in [9]. Moreover, we are able to enumerate the zero-energy edge modes by using an *index theorem*, a variant of the Aharonov-Casher theorem for the 2D Dirac equation in a vector potential [14]. Finally, we show that a lattice counterpart of this continuum model, including the anomalous edge modes, can be realized using honeycomb-like arrays of ring resonators with non-Hermitian couplings [15, 16].

Non-Hermitian Hamiltonian. — Our model is based on the following non-Hermitian Hamiltonian, defined on a

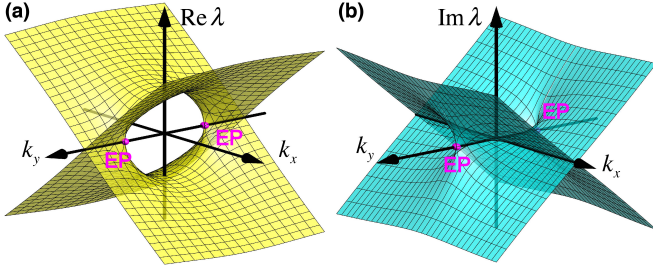


FIG. 1: Real and imaginary parts of the complex spectrum (2) of the Hamiltonian (1) with exceptional points at $\mathbf{k}_{\text{EP}}^{\pm} = (0, \pm|m|)$.

2D momentum space $\mathbf{k} = (k_x, k_y)$:

$$\hat{H} = \begin{pmatrix} k_x - isk_y & m \\ m & -k_x + isk_y \end{pmatrix} \quad (1)$$

$$\equiv (k_x - isk_y)\hat{\sigma}_z + m\hat{\sigma}_x \equiv \mathbf{B} \cdot \hat{\boldsymbol{\sigma}}.$$

Here, $\hat{\boldsymbol{\sigma}} = (\hat{\sigma}_z, \hat{\sigma}_x, \hat{\sigma}_y)$ denotes the vector of Pauli matrices (permuted cyclically for later convenience), and $\mathbf{B} = (B_x, B_y, 0)$ is an effective complex “magnetic field”, which will be used in the subsequent Berry-phase analysis. The Hamiltonian \hat{H} contains three continuously-tunable real parameters: the momenta k_x and k_y , and m (assumed real), which mixes the two spinor components, and which we call “mass” for convenience. The parameter $s = \pm 1$, which we will regard as a “non-Hermitian charge”, determines the sign of the imaginary part, such that $[H(s)]^\dagger = H(-s)$.

The Hamiltonian (1) involves only two Pauli matrices, and has the chiral symmetry $\{\hat{H}, \hat{\sigma}_y\} = 0$. It has eigenvalues

$$\lambda^{\pm} = \pm\sqrt{\mathbf{B} \cdot \mathbf{B}} = \pm\sqrt{m^2 + (k_x - isk_y)^2}, \quad (2)$$

and (non-normalized) eigenvectors

$$\psi^{\pm} = \begin{pmatrix} 1 \\ B_y/(B_x + \lambda^{\pm}) \end{pmatrix}. \quad (3)$$

The complex spectrum (2) is shown in Fig. 1. Along the k_y axis, the real part of the spectrum, $\text{Re}(\lambda)$ is gapped for $-|m| < k_y < |m|$, and ungapped for $|k_y| > |m|$. There are two EPs at $\mathbf{k}_{\text{EP}} = (0, \pm|m|)$, separating the “gapped” and “ungapped” k_y -domains.

Unlike Hermitian degeneracies, EPs involve the coalescence of eigenvectors, not just eigenvalues $\lambda^{\pm}(\mathbf{k}_{\text{EP}}) = 0$. $\hat{H}(\mathbf{k}_{\text{EP}})$ is defective and has a single chiral eigenmode (an eigenvector of $\hat{\sigma}_y$) [4, 17]

$$\psi(\mathbf{k}_{\text{EP}}) = \begin{pmatrix} 1 \\ i\chi_{\text{EP}} \end{pmatrix}, \quad (4)$$

where $\chi_{\text{EP}} = \pm \text{sgn}(sm)$ is the chirality of the EP.

Chiral edge modes.— We now translate Eq. (1) to a Schrödinger wave equation by taking $\hat{\mathbf{k}} = -i\nabla$ and allowing the mass m and/or non-Hermitian charge s to

vary with position (though we still assume that s only takes the values ± 1):

$$\hat{H} = [-i\partial_x - s(x, y)\partial_y]\hat{\sigma}_z + m(x, y)\hat{\sigma}_x. \quad (5)$$

Consider an interface between two uniform media with different m and/or s . For now, let the interface be along the line $x = 0$, such that $m = m_1$, $s = s_1$ for $x < 0$ (medium 1), and $m = m_2$, $s = s_2$ for $x > 0$ (medium 2). We seek edge modes that propagate along y and are normalizable along x :

$$\psi_{\text{edge}} = \begin{pmatrix} \alpha \\ \beta \end{pmatrix} \begin{cases} e^{iky + \kappa_1 x}, & \text{Re}(\kappa_1) < 0, \quad x > 0 \\ e^{iky + \kappa_2 x}, & \text{Re}(\kappa_2) > 0, \quad x < 0 \end{cases} \quad (6)$$

Substituting Eq. (6) into Eq. (5), we find the *zero-energy edge modes*, $\lambda_{\text{edge}} = 0$, which exist when the following real equations are satisfied:

$$-\kappa_1 = s_1 k \pm m_1, \quad -\kappa_2 = s_2 k \pm m_2. \quad (7)$$

For $\kappa_1 < 0$ and $\kappa_2 > 0$, there can be zero, one, or two solutions to Eq. (7) for each k . The number of solutions also depends on $m_{1,2}$ and $s_{1,2}$. Like the eigenmodes at the EPs of the bulk system, these edge modes are *chiral*, satisfying $\beta/\alpha = \pm i$. Similar to Eq. (4), we define the mode chirality as $\chi_{\text{edge}} = \text{Im}(\beta/\alpha)_{\text{edge}}$.

We first examine the two simplest cases:

(A) The media have equal charges, $s_1 = s_2 = s$, and opposite masses, $m_1 = -m_2 = m$. In this case, there is *one* zero-energy edge mode for each $k \in (-|m|, |m|)$, and no edge modes for all other k . This k -range corresponds to the k_y -domain with the *gapped* bulk spectra $\text{Re}(\lambda^{\pm})$ between the two EPs (Fig. 1). The mode chirality is $\chi_{\text{edge}} = \text{sgn}(m)$, independent of s . Note that this domain includes $k = 0$, which is the *Hermitian* limit where Eq. (5) reduces to the *Jackiw-Rebbi* model for 1D Dirac modes [11]. Thus, this is a family of non-Hermitian edge modes that are continuable from the Hermitian Jackiw-Rebbi edge modes.

(B) The media have equal “masses”, $m_1 = m_2 = m$, but opposite “charges”, $s_1 = -s_2 \equiv s$. In this case, there are *two* edge modes in the domain $k \in \text{sgn}(s)(|m|, \infty)$. This corresponds to one of the k_y domains with the *ungapped* $\text{Re}(\lambda^{\pm})$ bulk spectra. The two edge modes have opposite chiralities, $\chi_{\text{edge}} = \pm 1$, and are independent of m . Unlike case (A), these modes are essentially *non-Hermitian*. First, they are asymmetric in k , and do *not* exist in the Hermitian limit $k = 0$. Second, these modes are *defective*: the corresponding left eigenvectors (right eigenvectors of $\hat{H}(-k) = \hat{H}^\dagger(k)$) do not exist.

When $|m_1| \neq |m_2|$, the situation is more complicated. Figure 2 shows the edge modes for varying m_2 , with $s_1 = s_2 = 1$ and $m_1 > 0$. For $m_2 > m_1$, there is one edge mode for each $k \in (m_1, m_2)$, as shown in Fig. 2(a). For $m_2 < m_1$, there is one edge mode for each $k \in (-m_1, -m_2)$, as shown in Fig. 2(b)–(d); this includes

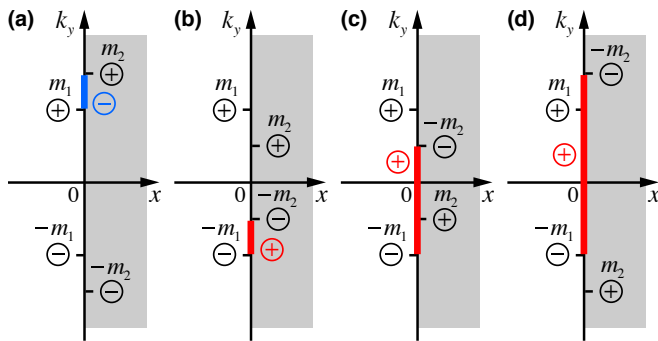


FIG. 2: Schematic diagrams indicating the zero-energy chiral edge modes (6) and (7) at the interface $x = 0$ between two media with different “masses” $m_1 > 0$ and m_2 , and the same “non-Hermitian charges” $s_1 = s_2 = 1$. Exceptional points \mathbf{k}_{EP} are indicated for the two media, with chiralities χ_{EP} marked by the black “+” and “-” signs. The edge modes with positive and negative chiralities χ_{edge} are marked by red and blue colors.

the special case (A) discussed above. For certain values of k , $\text{Re}(\lambda^\pm)$ is gapped in one medium and ungapped in the other medium. We call such zones and the corresponding edge modes “mixed”. When $m_2 > 0$, there are only positive or only negative values of k , as shown in Fig. 2(a),(b). In Fig. 2, we also indicate the chiralities of the EPs in the two media, χ_{EP} , and the chiralities of the edge modes, χ_{edge} . Remarkably, the edge modes always connect a pair of EPs with the same chirality, while the modes themselves have the opposite chirality.

We can summarize the conditions under which zero-energy edge modes exist using the phase diagrams in Fig. 3. Here, we fix $m_1 > 0$ and $s_1 = 1$, and use k/m_1 and m_2/m_1 as the plot axes. The red (blue) regions show where there is a single edge mode with $\chi_{\text{edge}} = +1$ ($\chi_{\text{edge}} = -1$). Figure 3(a) shows the case where the two media have equal non-Hermitian charge s , with the special case (A) lying on the $m_2/m_1 = -1$ line and 1D Jackiw-Rebbi model [11] lying on the $k = 0$ line. Figure 3(b) shows the opposite-charge case; it also contains a purple region indicating two edge modes with $\chi_{\text{edge}} = \pm 1$, which includes the case (B) on the line $m_2/m_1 = 1$.

We will now show that these phase diagram features—i.e., the number of zero-energy edge modes and under what conditions they appear—can be understood from the topological properties of Eq. (1).

Winding numbers.— Since some edge modes of our non-Hermitian model can be continued to Jackiw-Rebbi modes [11], and the termination points of the edge modes are the EPs of the bulk spectrum, we can guess that the edge modes can be characterized by bulk *topological invariants* [1, 18]. Along a 1D interface, the conserved k_y plays the role of a tunable parameter for calculating a 1D winding number. However, it turns out that *two* distinct

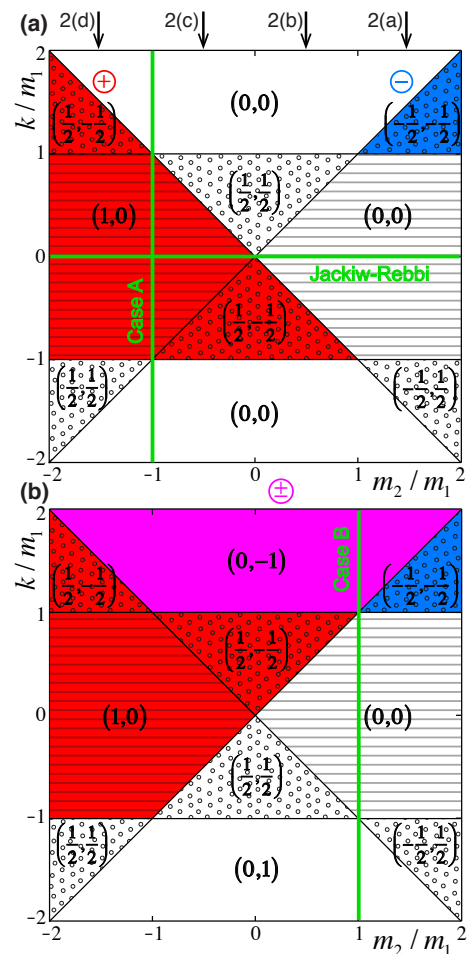


FIG. 3: Phase diagrams for the chiral edge modes (6) and (7) at the interface between two media with (a) equal “non-Hermitian charges” $s_1 = s_2 = 1$, and (b) opposite “charges” $s_1 = -s_2 = 1$. The “mass” in medium 1 is fixed as $m_1 > 0$. The arrows above (a) indicate the cases shown in Fig. 2. The numbers in parentheses indicate the differences of winding numbers (9) and (11) between the two media: $(\Delta w_1, \Delta w_2)$. Striped, empty, and dotted zones indicate gapped, ungapped, and mixed cases of the bulk spectra $\text{Re}(\lambda^\pm)$ in the two media.

winding numbers are needed to fully describe the edge modes in the non-Hermitian case.

Previous researchers [5, 6, 9, 19] have focused on the winding numbers of the eigenvectors ψ^\pm . However, we emphasize that encircling an EP (branch point) swaps the bands, so that *two* loops in parameter space are required to return to the original state (with a π geometric phase gained) [4, 9, 19, 20]. Hence, there is no globally smooth way to define two distinct bands for Eq. (3).

One way to resolve this band-labelling ambiguity is to consider winding numbers associated with the complex “magnetic field” \mathbf{B} defined in Eq. (1), which has no discontinuities. We introduce polar coordinates $\mathbf{B} = \lambda_\pm (\sin \theta \cos \phi, \sin \theta \sin \phi, \cos \theta)$, where θ and ϕ are complex [21]. In our case, \hat{H} has chiral symmetry, so \mathbf{B} is

constrained to the $\theta = \pi/2$ plane, and only evolution in ϕ takes place, with winding number

$$w_1 = \frac{1}{2\pi} \int_{\phi_+}^{\phi_-} d\phi, \quad (8)$$

where $\phi_{\pm} = \phi(k_x = \pm\infty)$. This is equivalent to the 1D winding numbers based on Berry phase used in Refs. [5, 6, 19]. For the Hamiltonian (1), we obtain

$$w_1 = \begin{cases} -\frac{1}{2}\text{sgn}(m), & \text{for } |k| < |m| \\ 0, & \text{for } |k| > |m| \end{cases} \quad (9)$$

This explains the edge modes in case (A), corresponding to the $m_2/m_1 = -1$ line in Fig. 3(a). Here, the difference in the topological numbers of the two media is $\Delta w_1 = w_1(m_2) - w_1(m_1) = \text{sgn}(m_1)$; accordingly, we observe a single edge mode of chirality $\chi_{\text{edge}} = \text{sgn}(m_1)$.

For other parameter choices, Δw_1 is fractional. In the case of Fig. 2(a) we find $\Delta w_1 = -1/2$, and for Fig. 2(b) $\Delta w_1 = 1/2$. These edge modes resemble the ‘‘anomalous’’ edge modes found in [9]. Clearly, the topological number w_1 is insufficient to characterize these modes, which are asymmetric in k .

To proceed, note that $\mathbf{B}(k_x = -\infty) = -\mathbf{B}(k_x = \infty)$. In the ‘‘gapped’’ Hermitian limit, $\mathbf{B} \cdot \mathbf{B} > 0$, and this requires $\Delta\phi = \pi$, so w_1 must be fractional. In the non-Hermitian case, this is not the only possibility: crossing a branch cut of λ^{\pm} changes the sign of \mathbf{B} while $\Delta\phi = w_1 = 0$ remains trivial. For $\mathbf{B} \neq 0$, there are two ways for λ_{\pm} to change sign: by encircling the origin of the complex plane in either a clockwise or anti-clockwise direction. This corresponds to two inequivalent EPs for each w_1 , distinguished by energy surfaces $\lambda^{\pm} \sim \sqrt{r} \exp(\pm is\theta/2)$ with chirality determined by s . These EPs can be distinguished by a second winding number,

$$w_2 = \frac{1}{2\pi} \int d\mathbf{k} \cdot \nabla_{\mathbf{k}} \text{Arg}(\lambda^{\pm}), \quad (10)$$

which counts the (signed) number of encircled branch points, divided by 2. This winding number is specific to complex spectra. For the spectrum (2), this yields

$$w_2(k_y) = \begin{cases} -\frac{1}{2}\text{sgn}(sk_y), & |sk_y| > |m| \\ 0, & |sk_y| < |m| \end{cases} \quad (11)$$

which has the required asymmetry in k_y . Whenever $w_2 \neq 0$, there are branch cuts in λ^{\pm} , and \hat{H} cannot be continuously deformed into a gapped Hermitian system.

Using Δw_1 and Δw_2 , we can completely characterize the edge modes shown in Fig. 3. First, for $w_2 = 0$, the existence of ‘‘Hermitian-like’’ edge modes (and their chirality) is determined by Δw_1 . Second, for $\Delta w_2 \neq 0$, the number of anomalous (‘‘non-Hermitian’’

and ‘‘mixed’’) edge modes is $2|\Delta w_2|$, while $\text{sgn}(\Delta w_2)$ determines whether they are localized to the left or right edge of medium 1. In Fig. 3, the anomalous non-Hermitian edge modes only exist on the right edge when $\Delta w_2 < 0$. In particular, the purple region in Fig. 3(b) corresponds to $\Delta w_2 = -1$, and accordingly there are two anomalous edge modes with opposite chiralities ($\Delta w_1 = 0$), and both are defective. Thus, the winding numbers $w_{1,2}$ provide the bulk-edge correspondence for the non-Hermitian Hamiltonian (5) and describe topological properties of the edge modes Fig. 3.

Since the topological numbers $w_{1,2}$ only change when k_y crosses an EP, we can identify the ‘‘topological charges’’ of the individual EPs as $(q_1, q_2) = \frac{1}{2}(\pm|m|, s)$. There are *four* inequivalent non-Hermitian degeneracies, in contrast to the *two* inequivalent Hermitian degeneracies. This is a consequence of the richer morphologies of complex vector fields that parametrize non-Hermitian Hamiltonians [22].

Index theorem.— Another way to analyze the zero-energy modes (zero modes) of the non-Hermitian Hamiltonian (5) is to consider the Hermitian Hamiltonian

$$\hat{\mathcal{H}} = \hat{H}^{\dagger} \hat{H}. \quad (12)$$

Zero modes of \hat{H} are also zero modes of $\hat{\mathcal{H}}$, and vice versa. When $s = \pm 1$ is a constant, we find that

$$\hat{\mathcal{H}} = |-i\nabla - \hat{\sigma}_y s \mathbf{A}(x, y)|^2 + \hat{\sigma}_y B(x, y), \quad (13)$$

where $B(x, y) = \partial_x A_y - \partial_y A_x$ and $\mathbf{A} = (0, m)$. This is a Pauli-type Hamiltonian for a nonrelativistic particle in a matrix-valued vector potential [23].

The normalizable zero modes of $\hat{\mathcal{H}}$ can now be counted by an ‘‘index theorem’’ argument [14]. The result is that there are $N = \lfloor |\Phi|/2\pi \rfloor$ such modes, where Φ is the total flux of B . This holds for *arbitrary* complex analytic mass fields $m(x, y)$. For the previously-considered special case of two media with a straight interface, there is a flux of $(m_2 - m_1)$ per unit length along the domain wall, and this implies that the zero modes occupy a k -range of $\Delta k = m_2 - m_1$, in precise agreement with Fig. 2 and Fig. 3(a) (see details in [16]).

Discussion.— We have analyzed a 2D non-Hermitian continuum model that exhibits different types of zero-energy edge modes, which can be classified using two half-integer-valued winding numbers calculated from the complex bulk band structure. These are inherently associated with topological properties of bulk eigenmodes and non-Hermitian degeneracies (EPs) in the band structure. One family of the edge modes includes the well known (Hermitian) Jackiw-Rebbi zero modes [11]. However, the classification also contains essentially non-Hermitian edge modes that cannot be continued into Jackiw-Rebbi-type edge modes; these seem to be continuum counterparts of the ‘‘anomalous’’ edge modes recently encountered in various 1D non-Hermitian lattice models [8, 9].

Importantly, non-Hermitian topological edge modes can be realized in 2D photonic ring resonator lattices, with non-Hermiticity introduced through either asymmetric scattering between clockwise and anticlockwise modes [2, 8], or by amplifying/lossy inter-resonator coupling. In the Supplementary Materials [16], we show that certain orientations of the lattice and interface yield fractional winding numbers and bands of zero energy edge modes.

We have mainly focused on the case of two uniform media separated by the line $x = 0$. However, for other orientations of the straight interface, we obtain similar phase diagrams, with $k = \mathbf{k} \cdot \hat{\mathbf{y}}$ where \mathbf{k} is the wavevector parallel to the interface. The index-theorem derivation of the number of normalizable zero modes is even more general, and applies to arbitrary mass fields.

The above features and comparison with previously-known examples suggest that the variety of chiral edge modes and topological numbers found in this work are generic for a very wide class of non-Hermitian wave systems.

The idea of this research was conceived by K.Y.B., C.Y.D., and D.L. at the workshop “Topological States of Light and Beyond” in the Center for Theoretical Physics of Complex Systems, Institute for Basic Science, Daejeon, South Korea. We are grateful to A. Miroshnichenko, A. B. Khanikaev, and S. Flach for their hospitality and inspiring discussions. This research was supported by the Singapore National Research Foundation (grant NRFF2012-02), the Singapore MOE Academic Research Fund Tier 2 (grant MOE2015-T2-2-008), the RIKEN iTHES Project, the MURI Center for Dynamic Magneto-Optics via the AFOSR (grant FA9550-14-1-0040), Grant-in-Aid for Scientific Research (A), the John Templeton Foundation, and the Australian Research Council.

-
- [1] M. Z. Hasan and C. L. Kane, *Rev. Mod. Phys.* **82**, 3045 (2010); X.-L. Qi and S.-C. Zhang, *Rev. Mod. Phys.* **83**, 1057 (2011); L. Lu, J.D. Joannopoulos, and M. Soljacic, *Nature Photon.* **8**, 821 (2014).
- [2] N. Moiseyev, *Non-Hermitian Quantum Mechanics* (Cambridge Univ. Press, 2011); C. M. Bender, *Rep. Prog. Phys.* **70**, 947 (2007); H. Cao and J. Wiersig, *Rev. Mod. Phys.* **87**, 61 (2015).
- [3] M. Goerbig and G. Montambaux, *Seminaire Poincare* **17**, 1 (2013) (arXiv:1410.4098); D. Leykam and A.S. Desyatnikov, *Advances in Physics: X* **1**, 101 (2016).
- [4] W.D. Heiss, *J. Phys. A: Math. Theor.* **45**, 444016 (2012); M.V. Berry, *Czech. J. Phys.* **54**, 1039 (2004).
- [5] M. S. Rudner and L. S. Levitov, *Phys. Rev. Lett.* **102**, 065703 (2009).
- [6] K. Esaki, M. Sato, K. Hasebe, and M. Kohmoto, *Phys. Rev. B* **84**, 205128 (2011).
- [7] Y. C. Hu and T. L. Hughes, *Phys. Rev. B* **84**, 153101 (2011).
- [8] H. Schomerus, *Opt. Lett.* **38**, 1912 (2013); S. Malzard, C. Poli, and H. Schomerus, *Phys. Rev. Lett.* **115**, 200402 (2015).
- [9] T.E. Lee, *Phys. Rev. Lett.* **116**, 133903 (2016).
- [10] S. Diehl *et al.*, *Nature Phys.* **7**, 971 (2011); J.M. Zeuner *et al.*, *Phys. Rev. Lett.* **115**, 040402 (2015); C. Yuce, *Phys. Lett. A* **379**, 1213 (2015); P. San-Jose *et al.*, *Sci. Rep.* **6**, 21427 (2016); M.S. Rudner, M. Levin, and L.S. Levitov, arXiv:1605.07652 (2016).
- [11] R. Jackiw and C. Rebbi, *Phys. Rev. D* **13**, 3398 (1976); S.-Q. Shen, W.-Y. Shan, and H.-Z. Lu, *SPIN* **1**, 1 (2011).
- [12] A.P. Schnyder, S. Ryu, A. Furusaki, and A.W.W. Ludwig, *Phys. Rev. B* **78**, 195125 (2008).
- [13] W.P. Su, J.R. Schrieffer, and A. J. Heeger, *Phys. Rev. Lett.* **42**, 1698 (1979); A.Y. Kitaev, *Phys.-Uspekhi* **44**, 131 (2001).
- [14] Y. Aharonov and A. Casher, *Phys. Rev. A* **19**, 2461 (1979).
- [15] S. Longhi, D. Gatti, G. Della Valle, *Phys. Rev. B* **92**, 094204 (2015).
- [16] See Supplementary Online Materials.
- [17] W. D. Heiss and H. L. Harney, *Eur. Phys. J. D* **17**, 149 (2001); C. Dembowski *et al.*, *Phys. Rev. Lett.* **90**, 034101 (2003); B. Peng *et al.*, *PNAS* **113**, 6845 (2016).
- [18] D.J. Thouless, *Topological Quantum Numbers in Nonrelativistic Physics* (World Scientific, 1998).
- [19] A. A. Mailybaev, O. N. Kirillov, and A. P. Seyranian, *Phys. Rev. A* **72**, 014104 (2005).
- [20] C. Dembowski *et al.*, *Phys. Rev. E* **69**, 056216 (2004); T. Gao *et al.*, *Nature* **526**, 554 (2015).
- [21] J. C. Garrison and E. M. Wright, *Phys. Lett. A* **128**, 177 (1988).
- [22] M. R. Dennis, K. O’Holleran, and M. J. Padgett, *Prog. Opt.* **53**, 293 (2007).
- [23] R. Jackiw, *Phys. Rev. D* **29**, 2375 (1986).
- [24] P. Delplace, D. Ullmo, and G. Montambaux, *Phys. Rev. B* **84**, 195452 (2011).

SUPPLEMENTARY ONLINE MATERIALS

Tight binding model

Here we consider a specific realization of fractional winding numbers in a ring resonator lattice. One important distinction between the continuum model studied in the main text and lattice models is the periodic boundary conditions imposed by the 2D Brillouin zone in the latter. To satisfy periodic boundary conditions, any branch cut in the eigenvalues must terminate at an inequivalent EP, such that $\sum q_2 = 0$. Therefore, regularizing Eq. (1) of the main text to a lattice will double the EP pairs, with the partners having opposite charges. To avoid cancellation of the total charge when integrating the 1D winding numbers, we can use a honeycomb lattice geometry such that each inequivalent K_{\pm} point generates a pair of inequivalent EPs and fractional winding numbers can occur for certain orientations of the lattice edge.

Specifically, we consider an anisotropic honeycomb lattice of ring resonators coupled by nonresonant link rings. Using a scheme such as the one introduced in [15], non-Hermitian couplings can be introduced by inserting gain and loss into the link rings to generate an imaginary gauge field described by a real asymmetric Hamiltonian. For simplicity, we introduce a non-Hermitian coupling into only one of the three links in Fig. 4. The Bloch Hamiltonian is

$$\hat{H} = \begin{pmatrix} 0 & ce^{\gamma} + e^{i\mathbf{k}\cdot\mathbf{a}_1} + e^{i\mathbf{k}\cdot\mathbf{a}_2} \\ ce^{-\gamma} + e^{-i\mathbf{k}\cdot\mathbf{a}_1} + e^{-i\mathbf{k}\cdot\mathbf{a}_2} & 0 \end{pmatrix}, \quad (14)$$

where c is the coupling strength in the y direction, γ is the imaginary gauge field strength, and the other two Hermitian couplings have been normalized to 1. Here, \mathbf{k} is the Bloch wavevector and the lattice vectors are $\mathbf{a}_1 = \frac{a}{2}(1, \sqrt{3})$, $\mathbf{a}_2 = \frac{a}{2}(-1, \sqrt{3})$, $\mathbf{a}_3 = a(1, 0) = \mathbf{a}_1 - \mathbf{a}_2$, where a is the lattice period. Note that \hat{H} has a chiral symmetry: $\{\hat{H}, \hat{\sigma}_z\} = 0$. For the bulk-edge correspondence to hold in a lattice, parity-time (\mathcal{PT}) symmetry was also required in [9]. Here \mathcal{T} is complex conjugation, $i \rightarrow -i$, and \mathcal{P} is a reflection about the x axis which maps $k_y \rightarrow -k_y$, $\mathbf{k} \cdot \mathbf{a}_1 \rightarrow -\mathbf{k} \cdot \mathbf{a}_2$, and $\mathbf{k} \cdot \mathbf{a}_2 \rightarrow -\mathbf{k} \cdot \mathbf{a}_1$. The Hamiltonian \hat{H} is parametrized by the two-component complex vector field

$$d_x = c \cosh \gamma + \cos(\mathbf{k} \cdot \mathbf{a}_1) + \cos(\mathbf{k} \cdot \mathbf{a}_2), \quad (15)$$

$$d_y = ic \sinh \gamma + \sin(\mathbf{k} \cdot \mathbf{a}_1) + \sin(\mathbf{k} \cdot \mathbf{a}_2). \quad (16)$$

In the Hermitian limit $\gamma = 0$, the isotropic ($c = 1$) lattice hosts Dirac points (Hermitian degeneracies) at the \mathbf{K} points, $\mathbf{K}_{\pm} = \frac{2\pi}{3a}(\pm 1, \sqrt{3})$. Reciprocal lattice vectors $\mathbf{G}_1 = \frac{2\pi}{a}(1, \frac{1}{\sqrt{3}})$, $\mathbf{G}_2 = \frac{2\pi}{a}(-1, \frac{1}{\sqrt{3}})$, $\mathbf{G}_3 = \frac{2\pi}{a}(1, 0)$ relate equivalent \mathbf{K} points. The anisotropy $c \neq 1$ shifts the Dirac points along the k_x axis (i.e. in the \mathbf{G}_3 direction) towards their partners. They merge and annihilate

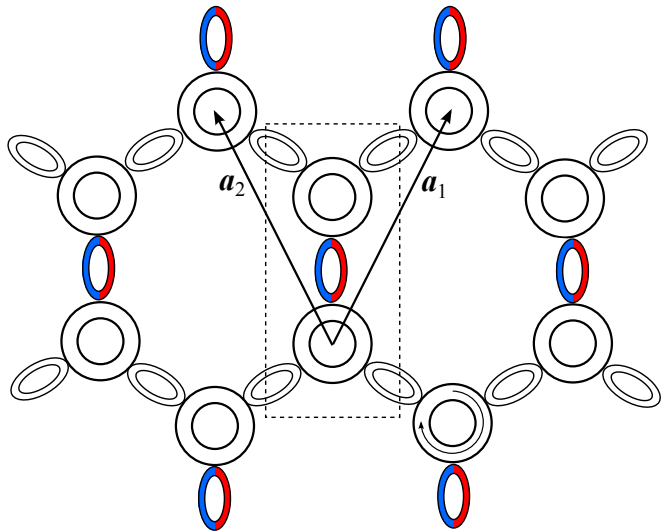


FIG. 4: Honeycomb lattice formed by ring resonators with gain/loss (red/blue) in one of the three link rings.

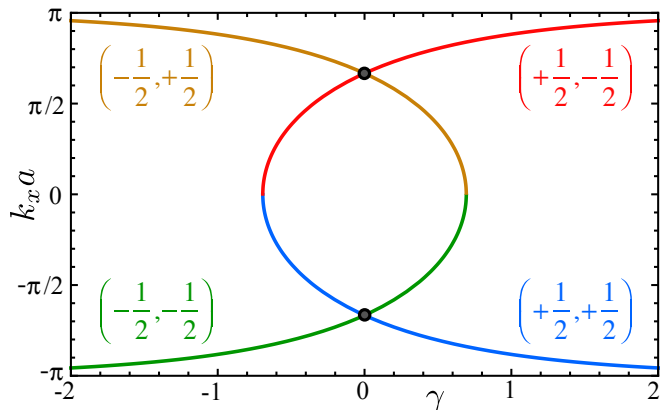


FIG. 5: Positions of exceptional points with charges (q_1, q_2) as a function of the non-Hermitian parameter γ . Black points indicate the Dirac points in the Hermitian limit $\gamma = 0$.

at the critical points $c = 0, 2$. A nonzero γ splits each Dirac point into a pair of EPs with charges (q_1, q_2) and positions

$$\left(+\frac{1}{2}, +\frac{1}{2}\right), \quad k_x = -2 \sec^{-1}\left(\frac{2e^{\gamma}}{c}\right), \quad (17)$$

$$\left(+\frac{1}{2}, -\frac{1}{2}\right), \quad k_x = 2 \sec^{-1}\left(\frac{2e^{\gamma}}{c}\right), \quad (18)$$

$$\left(-\frac{1}{2}, -\frac{1}{2}\right), \quad k_x = -2 \cos^{-1}\left(\frac{ce^{\gamma}}{2}\right), \quad (19)$$

$$\left(-\frac{1}{2}, +\frac{1}{2}\right), \quad k_x = 2 \cos^{-1}\left(\frac{ce^{\gamma}}{2}\right). \quad (20)$$

Figure 5 plots the EP positions as a function of γ (assuming $c = 1$). Note the vanishing total charge when EPs coalesce to form the Dirac points. On the other hand, when $\gamma \rightarrow \pm \ln \frac{c}{2}$ a different pair of EPs with $\sum q_1 = \pm 1$ and

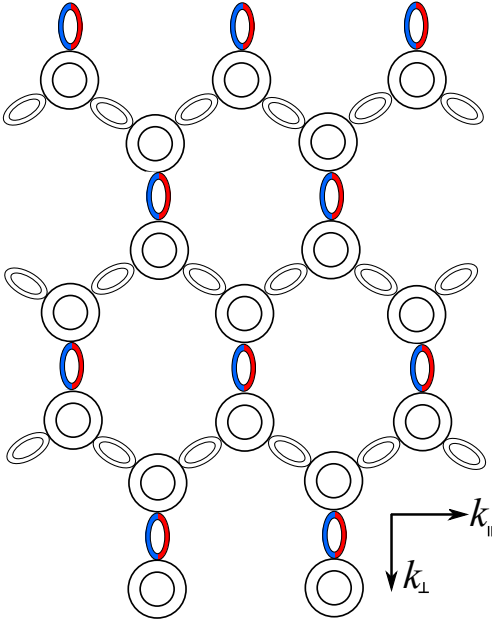


FIG. 6: Honeycomb lattice with “bearded” edge.

$\sum q_2 = 0$ merge and annihilate at $k_x = 0$. The remaining pair merges in the limit $\gamma \rightarrow \infty$ at $k_x = \pm \frac{\pi}{a}$. ($\gamma \rightarrow -\gamma$ swaps these merging points). Therefore by tuning (c, γ) we can control the relative positions and number of EPs in the bulk Hamiltonian. Note that the $m = 0$ limit of our continuum Hamiltonian Eq. (1) (coalescence of EPs with $\sum q_2 \neq 0$) is not realized in this model.

We now consider a lattice with “bearded” edges shown in Fig. 6. This edge termination respects both the chiral and \mathcal{PT} symmetries. To determine the resulting edge states, one must project $\mathbf{k} = k_{\parallel} \mathbf{e}_{\parallel} + k_{\perp} \mathbf{e}_{\perp}$ onto components parallel and perpendicular to the boundary, described by the reciprocal space basis vectors $\mathbf{e}_j = \mathbf{\Gamma}_j / |\mathbf{\Gamma}_j|$, with $\mathbf{\Gamma}_{\parallel} = \frac{2\pi}{a}(1, 0)$ and $\mathbf{\Gamma}_{\perp} = \frac{4\pi}{a\sqrt{3}}(0, -1)$ [24]. $k_{\parallel} \in \frac{\pi}{a}[-1, 1]$ becomes a parameter and the winding numbers of each domain are calculated over the 1D Brillouin zone defined by $k_{\perp} \in \frac{2\pi}{a\sqrt{3}}(-1, 1)$ using Eqs. (8) and (11). We verify that tuning $k_{\parallel} = k_x$ through the EPs in Fig. 5 changes the winding numbers by $\pm \frac{1}{2}$. Figure 7, for example, shows the calculated winding numbers as functions of k_{\parallel} when $\gamma = 0.2$, displaying k -intervals with $w_1 = 0, \frac{1}{2}, 1$ and $w_2 = 0, \frac{1}{2} \text{sgn}(\gamma)$. Therefore “bearded” edges or domain walls between regions with different $\gamma_1 \neq \gamma_2$ can host the non-Hermitian edge modes discussed in the main text.

To verify the existence of the predicted edge states, we numerically diagonalized \hat{H} on a semi-infinite strip with bearded edges. For sufficiently small k_x both edges support localized modes and they have opposite chiralities. Increasing k_x , one of the edge states becomes more strongly localized, while the other becomes more weakly localized, disappearing when the EP is crossed and $w_{1,2}$

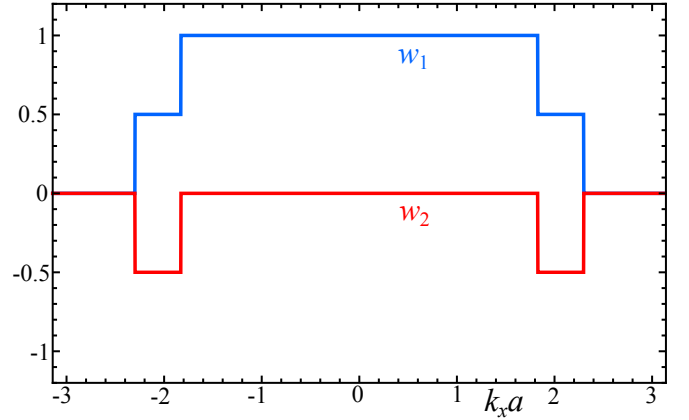


FIG. 7: Winding numbers w_1 and w_2 for a honeycomb lattice with bearded edges, as a function of $k_x = k_{\parallel}$. Here $c = 1$ and $\gamma = 0.2$ is the non-Hermitian coupling strength.

become fractional. The sole remaining edge state is defective, i.e. there are two zero energy eigenvalues sharing the same eigenvector.

This model also provides a simple way to understand the emergence of the anomalous edge states. For $\gamma > 0$, hopping in the $+\hat{y}$ direction is accompanied by amplification which will counteract the evanescent decay of a state localized to the lower edge, which delocalizes when the amplification rate exceeds the evanescent decay rate and ceases to exist. In contrast, hopping in the $-\hat{y}$ direction is accompanied by attenuation, which enhances the localization of the zero-energy states at the upper edge.

Counting zero modes with the index theorem

Given a non-Hermitian Hamiltonian \hat{H} , we can define the Hermitian Hamiltonian

$$\hat{\mathcal{H}} = \hat{H}^\dagger \hat{H}. \quad (21)$$

If $\hat{H}|\psi\rangle = 0$, then $\hat{\mathcal{H}}|\psi\rangle = 0$. Conversely, if $\hat{\mathcal{H}}|\psi\rangle = 0$, then $\langle \psi | \hat{H}^\dagger \hat{H} | \psi \rangle = 0$, which implies that $\hat{H}|\psi\rangle = 0$. Note that this holds for any choice of inner product, and does not rely on the eigenvectors of \hat{H} being orthogonal (they generally are not). Using the non-Hermitian Hamiltonian \hat{H} from Eq. (5), we obtain

$$\hat{\mathcal{H}} = (p_x - \hat{\sigma}_y s A_x)^2 + (s p_y - \hat{\sigma}_y A_y)^2 + \hat{\sigma}_y B(x, y) \quad (22)$$

where $p_i = -i\partial_i$, $\mathbf{A} = (s\text{Im}(m), \text{Re}(m))$, and $B(x, y) = \partial_x A_y - \partial_y A_x$.

Let us project to the eigenspace of $\hat{\sigma}_y$, thus replacing $\hat{\sigma}_y$ with $\sigma = \pm 1$. Now the zero modes of $\hat{\mathcal{H}}$ can be counted via a procedure originally introduced by Aharonov and Casher [14]. Define the canonical momentum operators

$$\pi_x = p_x - s\sigma A_x; \quad \pi_y = s p_y - \sigma A_y, \quad (23)$$

which obey the commutation relations $[\pi_x, \pi_y] = i\sigma B$. The Hermitian Hamiltonian $\hat{\mathcal{H}}$ can then be written as

$$\hat{\mathcal{H}} = (\pi_x + i\pi_y)(\pi_x - i\pi_y). \quad (24)$$

As we have argued above, a zero mode $|\psi\rangle$ must satisfy $(\pi_x - i\pi_y)|\psi\rangle = 0$. In terms of the wavefunction,

$$(-i\partial_x - s\partial_y - s\sigma A_x + i\sigma A_y)\psi(x, y) = 0. \quad (25)$$

Assuming $\nabla \cdot \mathbf{A} = 0$, we can let

$$A_x = \partial_y \phi, \quad A_y = -\partial_x \phi. \quad (26)$$

With this gauge choice, the magnetic field is the source of a potential ϕ :

$$\nabla^2 \phi(x, y) = B(x, y). \quad (27)$$

We substitute this back into Eq. (25), and make the further gauge substitution

$$\psi(x, y) = \exp[-\sigma\phi(x, y)]f(x, y). \quad (28)$$

Then $f(x, y)$ obeys

$$(\partial_x - is\partial_y)f(x, y) = 0. \quad (29)$$

In the first case of interest, $s_1 = s_2 = 1$, $f(x, y)$ is analytic in the complex plane, and hence cannot be normalized. Thus, the normalization of ψ must arise from the exponential factor in Eq. (28). Using Eq. (27), we write

$$\phi(r) = \int dr' G(r - r')B(r'), \quad (30)$$

$$G(r - r') = \frac{1}{2\pi} \ln\left(\frac{|r - r'|}{l_B}\right). \quad (31)$$

Here, l_B is the magnetic length that serves as the cut-off of the theory. For $r \gg r'$,

$$\phi(r) \rightarrow \ln\left(\frac{r}{l_B}\right)^{\Phi/2\pi}, \quad (32)$$

where

$$\Phi = \iint dx dy (\partial_x A_y - \partial_y A_x) = 2\pi(N + \epsilon). \quad (33)$$

Here, N is an integer and $0 < \epsilon < 1$. Substituting this back into Eq. (28), we arrive at

$$\psi(x, y) = \left(\frac{r}{l_B}\right)^{-\sigma\Phi/2\pi} f(x, y). \quad (34)$$

Next, we can expand the analytic function $f(x, y)$ with

$$f(x, y) = f(z) = z^j, \quad (35)$$

where $z = x + iy$. The resulting wave function is

$$\psi_j(z) = \left(\frac{|z|}{l_B}\right)^{-\sigma\Phi/2\pi} z^j. \quad (36)$$

For $\sigma\Phi > 0$, we require $j = 0, 1, 2, \dots, N - 1$, so that $\psi_j(z)$ is normalizable. For $\sigma\Phi < 0$, however, there are no normalizable zero modes. Thus, $\hat{\mathcal{H}}$ has a total of N zero modes. The zero modes are polarized either spin-up ($\sigma = +1$) or spin-down ($\sigma = -1$), depending on the sign of the total magnetic flux Φ . The flux Φ is determined by the mass profile $m(x, y) = m(z)$, which must be a complex analytic function according to Eq. (26).

In the second case, $s_1 = -s_2 = s$, $f(x, y) = f(z)$ is a piecewise-analytic function which can be decomposed in medium 1 using the Cauchy integral formula as

$$f(z) = \frac{1}{2\pi i} \oint \frac{f(t)}{t - z} dt, \quad (37)$$

where the integral is over the boundary between the two media. The analytic function $f^*(z)$ in medium 2 can be obtained similarly by requiring continuity of ψ at the interface. Since $f(z)$ is now normalizable, zero modes can exist even when the flux Φ vanishes, in which case they will be spin-degenerate. A nonzero flux Φ will generate an imbalance between the number of spin-up and spin-down modes.

Suppose now that $m = m(x)$ forms a straight domain wall in the vicinity of $x = 0$ with mass parameters $m_{1,2}$ in the limit $|x| \rightarrow \infty$. A straightforward calculation shows that $\phi(x) \rightarrow -m_1 x$, $\phi(x \rightarrow \infty) = -m_2 x$, the magnetic flux per unit length is $(m_2 - m_1)$, and $f(x, y) \propto \exp(-s_{1,2} kx +iky)$. The resulting wavefunction is

$$\psi(x, y) \sim \exp[iky - xs_{1,2}k - \sigma\phi(x)], \quad (38)$$

reproducing the condition for normalizable zero modes, Eq. (7), discussed in the main text.